spectroscopy journal

MDPI

Article

Conformational Analysis of Trifluoroacetyl Triflate, $CF_3C(O)OSO_2CF_3$: Experimental Vibrational and DFT Investigation

Agustín Spaltro, Melina G. Peluas, Carlos O. Della Védova and Rosana M. Romano *

Centro de Química Inorgánica "Dr. Pedro J. Aymonino", CEQUINOR (UNLP, CCT-CONICET La Plata, Associated with CIC-PBA), Departamento de Química, Facultad de Ciencias Exactas, Universidad Nacional de La Plata, Boulevard 120 N° 1465, La Plata CP 1900, Argentina; aspaltro@quimica.unlp.edu.ar (A.S.); mpeluas@quimica.unlp.edu.ar (M.G.P.); carlosdv@quimica.unlp.edu.ar (C.O.D.V.)
* Correspondence: romano@quimica.unlp.edu.ar

Abstract: The conformations of trifluoroacetyl triflate, $CF_3C(O)OSO_2CF_3$, were investigated through experimental vibrational methods (gas-phase FTIR, liquid-phase Raman, and Ar matrix FTIR spectroscopy) and density functional theory (DFT) calculations. A potential energy surface was computed using the B3P86/6-31+g(d) approximation as a function of the dihedral angles τ_1 = CC−OS and τ_2 = CO−SC. The surface reveals three minima, which were further optimized using the B3LYP method with various basis sets (6-31++G(d), 6-311++G(d), tzvp, and cc-pvtz). The global minimum corresponds to a *syn–anti* conformer (the C=O double-bound *syn* with respect the O−S single bond and the C−O single bond *anti* with respect to S−C single bond). The other two minima represent enantiomeric *syn–gauche* forms. The Ar matrix FTIR spectrum exhibited clear evidence of the presence of two conformers. Furthermore, the randomization process observed following broadband UV–visible irradiation facilitated the identification of the IR absorption of each conformer. Based on the Ar matrix FTIR experiments, the vapour phase of trifluoroacetyl triflate at room temperature was composed of approximately 60–70% of the *syn–anti* conformer and 30–40% of the *syn–gauche* form.

Keywords: conformations; matrix FTIR; gas-phase FTIR; Raman; DFT

check for updates

Citation: Spaltro, A.; Peluas, M.G.; Della Védova, C.O.; Romano, R.M. Conformational Analysis of Trifluoroacetyl Triflate, $CF_3C(O)OSO_2CF_3$: Experimental Vibrational and DFT Investigation. *Spectrosc. J.* **2024**, *2*, 68–81. https://doi.org/10.3390/spectroscj2020005

Academic Editors: Rui Fausto and Turrell Sylvia

Received: 24 April 2024
Revised: 1 June 2024
Accepted: 5 June 2024
Published: 8 June 2024

Copyright: © 2024 by the authors. Licensee MDPI, Basel, Switzerland. This article is an open access article distributed under the terms and conditions of the Creative Commons Attribution (CC BY) license (https://creativecommons.org/licenses/by/4.0/).

1. Introduction

Trifluoroacetyl triflate ($CF_3C(O)OSO_2CF_3$, TFAT) is a convenient reagent for trifluoroacetylation reactions in organic synthesis [1]. Its efficacy in trifluoroacylation reactions with various nucleophilic molecules, including alcohols [2], amines [2], aromatic activated substrates [3], covalent fluorides [4], and halides [5], among others, has been reported. However, TFAT's high reactivity imposes limitations on the choice of solvents for these reactions, with benzene, saturated hydrocarbons, and common halogenates solvents being among the few compatible options [1]. Despite its widespread use as a reagent and its availability from commercial sources, the structural and vibrational properties of trifluoroacetyl triflate remain unexplored, to the best of our knowledge.

Our group has successfully prepared molecules with the general formula $XC(O)OSO_2CF_3$, where X = F [6] or Cl [7,8], by reacting halocarbonylsulphenyl chloride, XC(O)SCl, with silver triflate salt, $AgSO_3CF_3$. These molecules exhibit an interesting conformational equilibrium. In the gas phase, $FC(O)OSO_2CF_3$ exists as a mixture of *anti* (the C−O single bond *anti* with respect to the S−C single bond) and *gauche* (the C−O double bond *gauche* with respect to the S−C single bond) forms. In both conformers the C=O double bond is *synperiplanar* with respect to the O-S single bond. Gas electron diffraction (GED) measurements revealed that the *syn–anti* rotamer predominates at ambient temperature, comprising 67(8)% of the gas-phase composition, whereas matrix FTIR estimated its presence at 59(5)% [6]. Similar results were obtained for $ClC(O)OSO_2CF_3$, with the *syn–anti* conformer constituting 66(8)% according to matrix FTIR measurements [7] and 67(11)% based on GED experiments [8]. Notably, $FC(O)OSO_2CF_3$ and $ClC(O)OSO_2CF_3$ are unique in exhibiting a prevailing *anti*

conformation around the S−O single bond, unlike other $XOSO_2CF_3$ species, which typically adopt a *gauche* conformation (see Refs. [6,8] and references cited therein). In this sense, a close and well-known example is the $ClC(O)OSO_2Cl$ molecule, where the *gauche* conformation predominates over the anti [9].

Matrix IR spectroscopy emerged as a valuable technique for investigating conformational equilibrium. Under such conditions, IR absorptions are narrowed compared to those observed in gas and condensed phases. This phenomenon primarily arises from the inhibition of rotation and intermolecular interactions in the isolated environment. Consequently, this method enables the discernment of bands with small wavenumber differences, being particularly useful in distinguishing spectral features between conformers.

The experimental setup employed in matrix formation ensures the preservation of the conformational composition existing at the temperature of the mixture prior to deposition. However, irradiating a compound isolated within a matrix can induce interconversion between conformers, leading to a randomization process. This results in a final state where the proportion of each conformer approximates 50%. This phenomenon was observed in FC(O)SBr isolated in matrices [10]. It was explained by a transition to an excited state, wherein the minimum in the potential curve as a function of the torsion angle coincides with the maximum of the energy surface in the ground state. Consequently, this leads to a decay with equal probability into the two conformers. This process has been observed for several other molecules (see, for example, Refs. [11–13], and references cited therein). This behaviour constitutes a very important tool for a clear assignment of the IR absorptions to each conformer.

In this work, we explored two distinct routes for synthesizing trifluoroacetyl triflate. The first route involved the reaction of trifluoroacetyl chloride with silver triflate, while the second route involved the reaction between trifluoroacetic and triflic acid. For the latter method, which has been reported in several works in the literature [2,14–16], we sought to optimize the conditions to yield a highly pure sample. We conducted a comprehensive analysis using various spectroscopic techniques. Specifically, we measured the FTIR spectra of the vapor phase, the Raman spectrum of the liquid phase, and the FTIR spectra of the sample isolated in solid argon immediately after deposition and at different intervals following broadband UV–visible irradiation. To provide theoretical insights, we employed density functional theory (DFT) methods to calculate a potential energy surface. Subsequently, we optimized the minima over this surface. The assignment of vibrational spectra and the experimental estimation of the proportion of conformers in the vapour phase at ambient temperature were carried out based on the Ar matrix FTIR spectra before and after irradiation, aided by predictions from theoretical calculations.

2. Materials and Methods

Chemicals: trifluoroacetic acid ($CF_3C(O)OH$, Carlo Erba, Emmendingen, Germany), phosphorus pentachloride (PCl_5, Sigma Aldrich, St Louis, MO, USA), silver triflate ($AgSO_3CF_3$, Fluka, Charlotte, NC, USA), and triflic acid ($HOSO_2CF_3$, Sigma Aldrich) were utilised without further purification. Ar (AGA) was purified by passing it through two U-traps. The first trap contained a thermally activated molecular sieve and the second was cooled to approximately −90 °C with an acetone bath to retain potential traces of impurities, primarily H_2O and CO_2.

The FTIR spectra were acquired using a Nexus Nicolet instrument, equipped with either a cryogenic mercury cadmium telluride (MCTB) or a deuterated triglycine sulfate (DTGS) detector for the ranges 4000–400 or 600–180 cm^{-1}, respectively. For vapour-phase IR studies at ambient temperature, a 10 cm gas cell fitted with CsI windows was employed.

Raman spectra were obtained using a Horiba-Jobin-Yvon T64000 Raman spectrometer (Horiba, Villeneuve-d'Ascq, France) equipped with a confocal microscope and a charged-coupled device (CCD) detector. Excitation was achieved using a 514.5 nm excitation wavelength from an Ar multiline laser. The wavenumbers were calibrated using the 459 cm^{-1} band of CCl_4. The net liquid sample was contained within a sealed capillary for ambient temperature measurements.

UV–visible spectra of gaseous samples were acquired using a Shimadzu UV-2600 (Shimadzu Corporation, Kyoto, Japan) spectrometer equipped with a double beam. The measurements were conducted with a 10 cm gas cell featuring quartz windows and a Young valve. An evacuated cell served as the background reference.

A 1 L vacuum flask was filled with TFAT and Ar in a proportion of 1:1000 using standard manometric techniques. The gas mixture was deposited onto a CsI window, cooled to approximately 15 K using a Displex closed-cycle refrigerator (SHI-APD Cryogenics, model DE-202, A S Scientific Products Ltd., Abingdon, UK) employing a pulse deposition technique. Matrix-isolated FTIR spectra were recorded in the 4000–400 cm^{-1} range using a Thermo Nicolet 6700 instrument (Thermo Fisher Scientific, Waltham, MA USA) equipped with a DTGS detector. The matrices were exposed to broadband UV– visible radiation ($200 \leq \lambda \leq 800$ nm) emitted by a Spectra-Physics Hg–Xe arc lamp operating at 1000 W. To mitigate heating effects, the lamp output was restricted by a water filter to absorb infrared radiation.

All of the quantum chemical calculations were conducted using the Gaussian 09 program system [17]. A relaxed potential energy surface was computed using the B3P86 functional (Becke three parameter hybrid functional with the non-local correlation provided by Perdew 86 [18]) in conjunction with the 6-31+G(d) basis set. Geometry optimizations of the energy minima employing the B3LYP method (Becke three parameter hybrid functional with the non-local correlation provided by Lee, Yang, and Parr [19,20]) and various basis set functions were sought using standard gradient techniques, allowing for simultaneous relaxation of all geometrical parameters. For comparison purposes, the optimization was also performed using the second-order Møller–Plesset perturbation theory (MP2) method in combination with the 6-31++G(d) basis set. Subsequently, these optimised structures were characterised via their vibrational properties. Natural Bond Orbital (NBO) analysis was performed for each structure and the orbital stabilization energies were calculated [21,22]. The electronic spectra for the previously optimized structures of both conformers were simulated using time-dependent density functional theory (TD-DFT) formalisms. Simulations were conducted with a maximum of 100 states and a spin multiplicity S = 1 [23,24].

3. Results and Discussion

3.1. Synthesis of Trifluoroacetyl Triflate (TFAT)

Trifluoroacetyl triflate, a colourless liquid at ambient temperatures, was synthetised via the reaction between trifluoroacetic acid and triflic acid, as illustrated in Scheme 1. Phosphorus pentoxide served as the dehydrating agent. These reactions were conducted at ambient temperature under an inert atmosphere, utilising either nitrogen or argon.

$$CF_3C(O)OH + HOSO_2CF_3 \xrightarrow[-H_2O]{P_2O_5} CF_3C(O)OSO_2CF_3$$

Scheme 1. Synthesis of trifluoroacetyl triflate.

The formation reaction of TFAT by this route competes with the dehydration of trifluoroacetic and triflic acids caused by phosphorus pentoxide, according to the reactions described in Scheme 2. Taking into account that the spectroscopic studies carried out in this work, particularly matrix-isolation spectroscopy, require highly pure samples, various stoichiometric ratios of the reagents were explored. This optimization aimed to minimize secondary reactions and ensure optimal conditions for the desired reactions.

$$2\ CF_3C(O)OH \xrightarrow[-H_2O]{P_2O_5} CF_3C(O)OC(O)CF_3$$

$$2\ HOSO_2CF_3 \xrightarrow[-H_2O]{P_2O_5} CF_3SO_2OSO_2CF_3$$

Scheme 2. Secondary reactions in the synthesis of trifluoroacetyl triflate.

TFAT undergoes hydrolysis at room temperature, yielding trifluoroacetic acid and triflic acid [1], as well as the two anhydrides depicted in Scheme 2. Due to its hydrophilicity, purification must be conducted in a moisture-free environment. Initially, the reaction between trifluoroacetic acid and triflic acid was carried out with an equimolar ratio of both acids, following previously reported conditions [1,14]. Under these reaction conditions, a high proportion of the $CF_3C(O)OC(O)CF_3$ anhydride relative to TFAT was obtained. Subsequently, experiments were conducted using a 2:1 ratio between trifluoroacetic and triflic acids, respectively, as described in existing literature [2,15]. However, these tests yielded even poorer results than the previous ones, since the proportion of trifluoroacetic anhydride with respect to TFAT was even higher in these conditions. This entails, as mentioned above, greater efforts in the purification process and consequently a decrease in the yield.

To minimise the formation of the $CF_3C(O)OC(O)CF_3$ anhydride, the reaction was conducted with a 1:2 ratio between trifluoroacetic and triflic acids. This ratio was chosen deliberately to favour the formation of the $CF_3SO_2OSO_2CF_3$ anhydride over the $CF_3C(O)OC(O)CF_3$ anhydride, which exhibits lower volatility (approximately 8 mbar at ambient temperature) and facilitates its subsequent separation from TFAT. The synthesis of the TFAT used for the spectroscopic studies presented in this work was carried out under these conditions, using an Ar atmosphere to mitigate potential hydrolysis reactions.

Efforts to synthesise trichloroacetyl triflate by reacting silver triflate with trifluoroacetyl chloride, aiming to eliminate water presence, were unsuccessful. Experimental details of this reaction are presented in the supplemental material.

3.2. Quantum Chemical Calculations

To identify different conformational isomers, we computed a potential energy surface as a function of two dihedral angles, τ_1 = O=C−O−S and τ_2 = C−O−S−C, as shown in Figure 1. T_1 was varied from −180 to 180° in steps of 10°, while τ_2 was varied from 0 to 360°, also in steps of 10°. The energy at each data point was determined using the B3P86/6-31+g(d) approximation, while all geometric parameters were simultaneously optimized, except for the torsion angles τ_1 and τ_2.

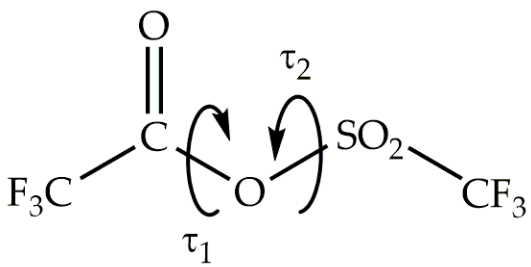

Figure 1. Definition of the dihedral angles τ_1 = O=C−O−S and τ_2 = C−O−S−C of trifluoroacetyl triflate.

Figure 2 displays the calculated potential energy surface (left panel) and the contour map (right panel). The global minimum is evident, corresponding to τ_1 = 0° and τ_2 = 180°. Moreover, the surface reveals two additional local minima, where τ_1 is approximately 0°, while τ_2 is around 70 and 290°, respectively. Subsequently, each of these minima underwent optimization using the B3LYP method with various basis functions, involving the simultaneous relaxation of all geometric parameters. The global energy minimum is denoted as the *syn–anti* conformer, characterised by the C=O double bound being *syn* with respect to the O−S single bond and the C−O single bond being *anti* with respect to the S−C single bond. The second is termed as the *syn–gauche*, where the C=O double bound is *syn* with respect to the O−S single bond and the C−O single bond is *gauche* with respect to the S−C single bond. The structures optimized with the B3LYP/cc-pvtz approximation present values of τ_1 = 0.0 and τ_2 = 180.0° for the global minimum. For the two more energetic enantiomeric forms, the values are τ_1 = −15.7 and τ_2 = 83.4°, and τ_1 = 15.7 and τ_2 = 276.6°.

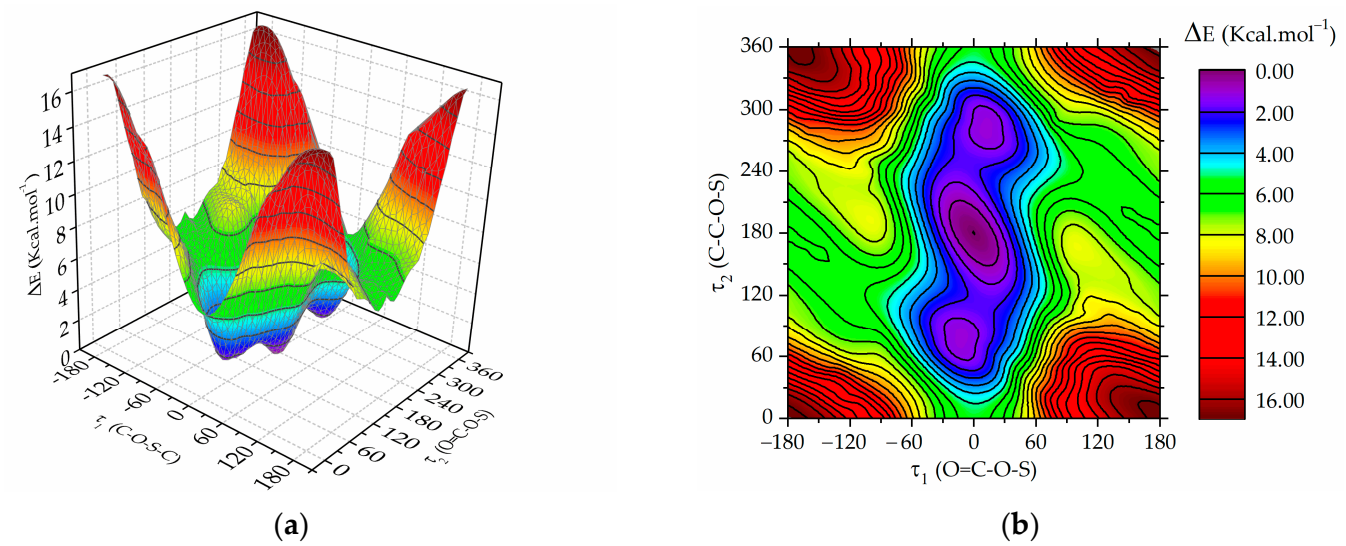

Figure 2. (**a**) Potential energy surface and (**b**) contour map computed with the B3P86/6-31+g(d) approximation as a function of the dihedral angles τ_1 = O=C−O−S and τ_2 = C−O−S−C of trifluoroacetyl triflate varied from −180 to 180° and from 0 to 360°, respectively, in steps of 10°.

Figure 3 exhibits the molecular models of the optimised structures for both rotamers of trifluoroacetyl triflate, computed using the B3LYP/cc-pvtz approximation. The geometrical parameters are detailed in Table S1 of the Supplementary Material, while the Cartesian coordinates for the *syn–anti* and *syn–gauche* conformers are provided in Tables S2 and S3, respectively. In all instances, energy minima devoid of imaginary frequencies were achieved. Furthermore, Table S4 presents a comprehensive compilation of calculated wavenumbers, IR and Raman intensities, along with a tentative assignment of vibrational modes for each conformer according to the B3LYP/cc-pvtz approximation.

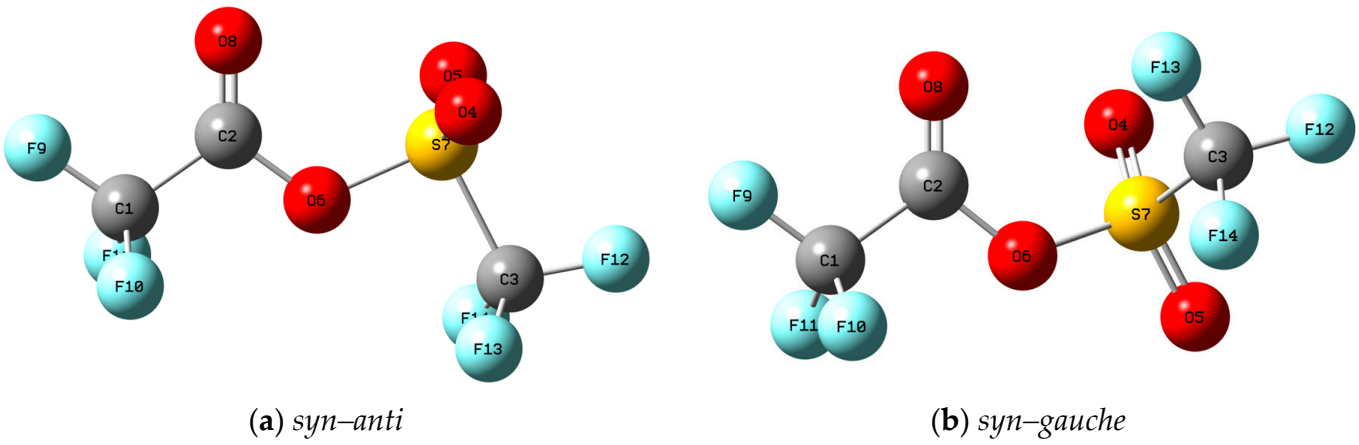

Figure 3. Molecular models of the conformers of trifluoroacetyl triflate computed with the B3LYP/cc-pvtz approximation: (**a**) *syn–anti* (the C=O double bond *syn* with respect to the O−S single bond and the C−O single bond *anti* with respect to the S−C bond); (**b**) *syn–gauche* (the C=O double bond *syn* with respect to the O−S single bond and the C−O single bond *gauche* with respect to the S−C bond).

Table 1 presents the energy differences and the Gibbs free energy differences between the *syn–gauche* and *syn–anti* conformers, calculated with B3LYP theoretical approximation with various basis sets, and also with the MP2/6-31++G(d) approximation. Additionally, the relative population of the rotamers at 25 °C was determined using the Boltzmann equation, considering a degeneracy of two for the *syn–gauche* form. The table reveals that, across all cases, the *syn–anti* form corresponds to the lowest energy conformer. However, the

computed percentage at room temperature fluctuates depending on the basis set utilized, ranging from 96 to 69%. The MP2 calculations predicted relative stabilities within this energy range. These findings will be discussed further along with the analysis of the experimental results.

Table 1. Energy differences and Gibbs free energy differences between *syn–gauche and syn–anti* conformers of trifluoroacetyl triflate and percentage of the *syn–anti* rotamer calculated with B3LYP theoretical approximation and different basis sets.

Theoretical Approximation	ΔE (Kcal·mol^{-1}) [1]	ΔG° (Kcal·mol^{-1}) [2]	% *syn–anti* [3]
B3LYP/6-31++G(d)	1.26	2.22	96
B3LYP/6-311++G(d)	1.23	2.02	94
B3LYP/tzvp	1.11	1.34	83
B3LYP/cc-pvtz	0.87	0.88	69
MP2/6-31++G(d)	0.70	0.98	72

[1] ΔE = E(*syn–gauche*) − E(*syn–anti*); [2] ΔG° = G°(*syn–gauche*) − G°(*syn–anti*); [3] Calculated at ambient temperature (25 °C) and considering degeneracy two for the *syn–gauche* conformer.

To comprehensively understand the conformational preferences of TFAT, we conducted orbital interaction analyses using the natural bond orbital (NBO) formalism [21]. Table 2 summarizes the key NBO stabilization energies computed, encompassing both hyperconjugative and anomeric effects. The hyperconjugative effect involves the interaction between a non-bonding orbital with a π character, known as nπ(O), located on the oxygen atom (−O−), and the π antibonding orbital of the C=O double bond, referred to as π*(C=O). On the other hand, the *syn* conformation is stabilized by the anomeric effect corresponding to the lpσO → σ*C=O interaction. The *syn–anti* conformer is additionally stabilised by two lpσO → σ*S=O interactions, while for the *syn–gauche* form the lpσO → σ*S−C interaction emerges as the most significant factor contributing to its stabilization (see Table 2 for details). Figures S1 and S2 depicts a schematic representation of these orbital interactions. Upon analysis of the values presented in Table 2, it becomes evident that both hyperconjugative and anomeric effects play significant roles in stabilizing the *syn–anti* over the *syn–gauche* rotamer.

Table 2. Main orbital interaction energies (Kcal.mol $^{-1}$) involved in the stabilization of the *syn–anti* and *syn–gauche* conformers of trifluoroacetyl triflate, calculated with the NBO formalism using the B3LYP/cc-pvtz approximation.

Orbital Interaction [1]	*syn–anti*	*syn–gauche*
lpπO6 → π*C2=O8	39.20	35.65
lpσO6 → σ*C2=O8	7.20	7.48
lpσO6 → σ*S=O4	5.42	–
lpσO6 → σ*S=O5	5.42	–
lpσO6 → σ*S−C3	–	5.93
Total anomeric effect	18.04	13.41
Total hyperconjugative effect	39.20	35.65
Total	57.24	49.06

[1] Atom numbering refers to Figure 3.

The vibrational spectra (IR and Raman) of each TFTA conformer were simulated using the B3LYP theoretical approximation in conjunction with various basis sets. The results will be discussed in the following section, alongside the experimental findings.

The electronic spectra of the *syn–anti* and *syn–gauche* conformers were simulated with a TD-B3LYP/cc-pvtz approximation. Figure S3 in the Supplementary Material presents the calculated individual spectra for each rotamer, along with the weighted sum of both spectra. Only one very weak transition is predicted for each conformer in the experimental working range, which is above 200 nm. Table 3 lists the wavelength of these transitions, their oscilla-

tor strengths, and their assignment. Figures S4 and S5 provide schematic representations of the HOMO and LUMO orbitals for the *syn–anti* and *syn–gauche* forms, respectively.

Table 3. Calculated wavelength (nm), oscillator strength, and assignment of the electronic transitions of the *syn–anti* and *syn–gauche* conformers of trifluoroacetyl triflate above 200 nm, calculated with the TD-B3LYP/cc-pvtz approximation.

	syn–anti	***syn–gauche***
Wavelength (nm)	226	229
Oscillator strength	0.0013	0.0014
Assignment	HOMO → LUMO $lp_pO \rightarrow \pi^*C{=}O$	HOMO → LUMO $lp_pO \rightarrow \pi^*C{=}O$

3.3. Vibrational Studies

As stated in the introduction, to the best of our knowledge, there have been no prior vibrational studies conducted on trifluoroacetyl triflate reported in the literature. In this study, we conducted measurements and analyses of the FTIR spectra in the gas phase, the Raman spectrum in the liquid phase, and the FTIR spectra of matrix-isolated $CF_3C(O)OSO_2CF_3$. Our focus was particularly on identifying signals that could be attributed to different conformers. Figure 4 illustrates the experimental spectra, while Table 4 presents the experimental wavenumbers alongside the predicted values for the *syn–anti* and *syn–gauche* conformers, calculated using the B3LYP/cc-pvtz approximation, and a tentative assignment. For band assignment, we considered the following criteria: (i) theoretical predictions, especially differences in wavenumbers for the vibrational modes of each conformer; (ii) the behaviour of IR absorptions of TFAT isolated in an argon matrix following UV–visible irradiation; and (iii) comparison with reported values for molecules similar to TFAT.

Table 4. Experimental wavenumber (gas FTIR, Ar matrix FTIR, and liquid Raman) in cm^{-1} of trifluoroacetyl triflate, comparison with the calculated wavenumbers using the B3LYP/cc-pvtz approximation for the *syn–anti* and *syn–gauche* conformers, and tentative assignment.

Experimental [a]			**B3LYP/cc-pvtz** [c,d]		**Tentative Assignment**
Gas-FTIR ν (cm^{-1})	**Ar matrix FTIR ν (cm^{-1})** [b]	**Liquid Raman ν (cm^{-1})**	***syn–anti***	***syn–gauche***	
1852 m	1860 w 1845 w	1880 1851	 1882 (38)	1892 (37)	ν C=O *syn–gauche* ν C=O *syn–anti*
1465 m	1475 m 1453 m	1455	 1426 (35)	1434 (33)	ν_{as} SO_2 ***syn–anti*** ν_{as} SO_2 ***syn–gauche***
1314 w	1319 vw 1315 vw	1317	1301 (7)	 1293 (9)	ν C−CF_3 ***syn–anti*** ν C−CF_3 ***syn–gauche***
1252 s	1249 s 1248 s		1242 (35)	 1241 (64)	ν_{as} CF_3 (−SO_2) ***syn–anti*** ν_{as} CF_3 (−SO_2)***syn–gauche***
1241 s	1243 s 1241 s	1266	1236 (41)	 1234 (36)	ν_{as} CF_3 (−C=O) ***syn–anti*** ν_{as} CF_3 (−C=O) ***syn–gauche***
1234 sh	1236 m		1231 (31)	1231 (29)	ν_{as} CF_3 (−SO_2)
	1228 m	1254	1225 (27)	1225 (6)	ν_s SO_2 *syn–anti*
1204 m	1200 w 1196 m		 1179 (35)	1182 (44)	ν_{as} CF_3 (−C=O)***syn–gauche*** ν_{as} CF_3 (−C=O)***syn–anti***
1142 m	1136 s	1133	1106 (36)	1106 (42)	ν_s CF_3 (−SO_2)
1040 s	1047 m 1018 m		1061 (100)	 1043 (100)	ν C−O***syn–anti*** ν C−O***syn–gauche***
842 w	847 w 836 w	840	852 (15)	 843 (6)	δ OCO ***syn–anti*** δ OCO ***syn–gauche***

Table 4. *Cont.*

Experimental [a]			B3LYP/cc-pvtz [c,d]		Tentative Assignment
Gas-FTIR ν (cm^{-1})	**Ar matrix FTIR ν (cm^{-1}) [b]**	**Liquid Raman ν (cm^{-1})**	***syn–anti***	***syn–gauche***	
788 w	788 w 786 m	780	 765 (2)	774 (7)	$\delta_{o.o.p.}$ (C=O) ***syn–gauche*** $\delta_{o.o.p.}$ (C=O) ***syn–anti***
779 sh	780 vw		770 (<1)	770 (1)	ν_s CF_3 ($-SO_2$)
751 w 733 m	746 m 730 w	759	741 (9)	 734 (8)	δ_s CF_3 (−C=O) *syn–anti* δ_s CF_3 (−C=O) ***syn–gauche***
704 sh	705 vw	733	686 (46)	686 (46)	ν S−O
611 m	611 m 609 m		 587 (10)	594 (20)	ω SO_2 ***syn–gauche*** ω SO_2 *syn–anti*
600 w	601 w 598 w	585	 566 (8)	575 (7)	ν C−S ***syn–gauche*** ν C−S *syn–anti*
585 sh	580 vw		556 (<1)	554 (<1)	δ CF_3 ($-SO_2$)
566 vw	566 w	559	544 (1)	547 (<1)	δ CF_3 ($-SO_2$)
522 vw	521 vw		519 (1)	517 (<1)	δ CF_3 (−C=O)
498 w	496 m 492 w		489 (7)	 487 (10)	δ SO_2 *syn–anti* δ SO_2 *syn–gauche*
		438	432	428	δ O=S=O
		421	415	381	δ C−C=O
		330	325	335	δ F−C−C
		302	300	284	δ F−C−C
		276	257	277	δ F−C−S
		242	236	243	ω CF_3 (−C=O)
		202	186	200	δ C−O−S
		170	159	149	δ O−S−C

[a] sh: shoulder; s: strong; m: medium; w: weak; vw: very weak; [b] Only the most intense matrix sites are listed; [c] unscaled values; [d] relative IR intensities with respect to the most intense normal mode of each conformer between parentheses.

The expected differences between the IR spectra of both conformers were meticulously scrutinized based on the computationally simulated spectra. As shown in Table 4, certain vibrational modes are expected to exhibit nearly identical wavenumbers for both forms. Conversely, several vibrational modes display significant wavenumber disparities, enabling their distinct detection, particularly in the Ar matrix FTIR spectra, which feature narrower bands compared to the gas and liquid phase spectra. Figure 5 illustrates the plot of the IR spectra simulated using the B3LYP/cc-pvtz approximation for the *syn–anti* and *syn–gauche* conformers, each multiplied by the relative abundance calculated using the same theoretical approximation, as well as the weighted sum of the individual spectra. This plot highlights selected regions where appreciable wavenumber differences were observed. These simulated spectra were then compared with the experimental spectra, with particular emphasis on the Ar matrix FTIR spectrum, which served as a valuable tool for assignment purposes. Figure 6 compares the simulated IR spectra of both TFAT conformers with the FTIR spectrum of TFAT isolated in an Ar matrix. The comparison focuses on selected spectral regions where the differences in wave numbers between the bands assigned to each conformer are significant enough to allow clear identification. IR signals originating from different matrix sites can be observed in the experimental spectrum depicted in Figure 6.

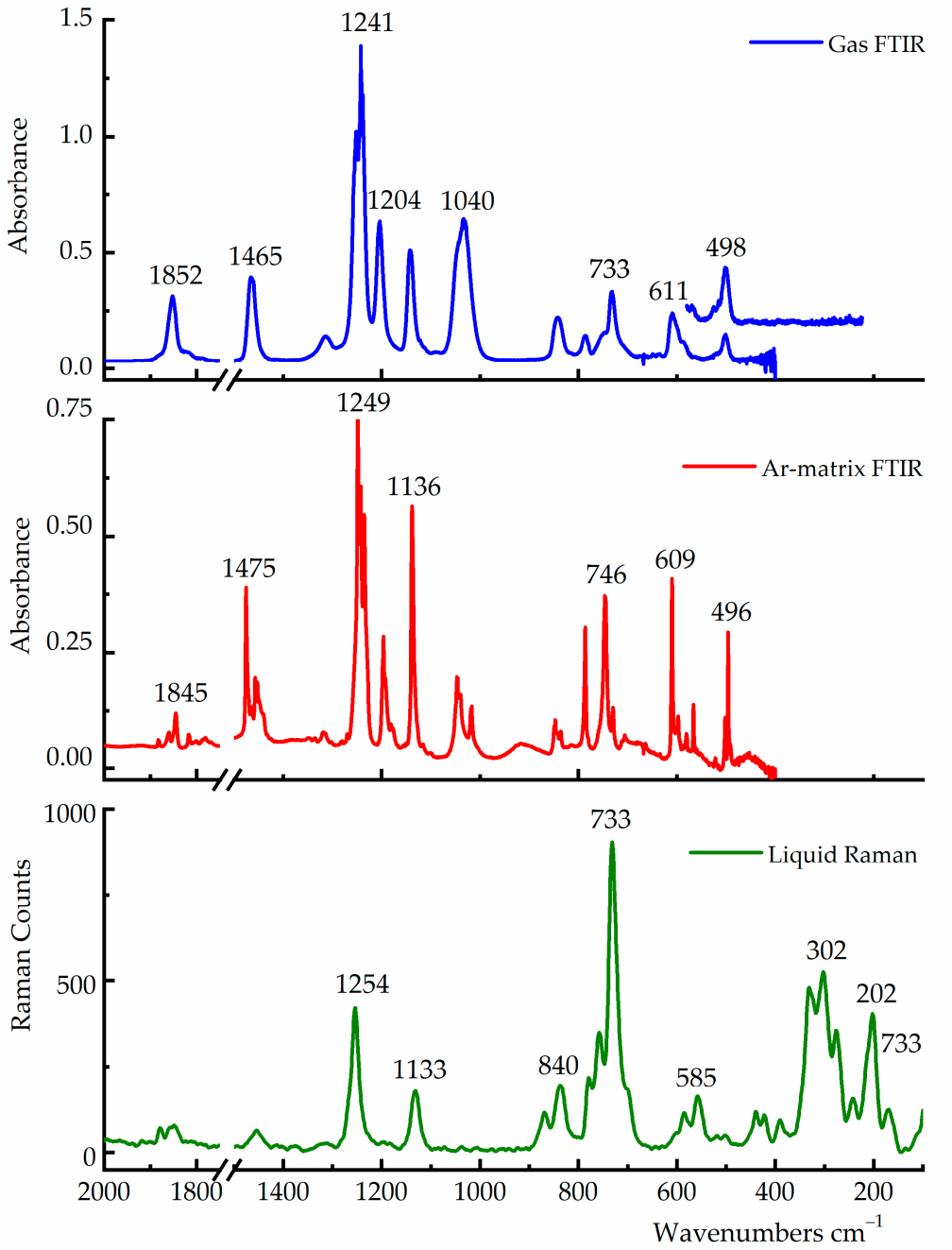

Figure 4. Gas-phase FTIR spectrum (blue trace, pressure 1.7 mbar, 0.5 cm^{-1} resolution, 64 scans), Ar matrix FTIR spectrum (red trace, 1:1000, 0.5 cm^{-1} resolution, 256 scans), and liquid-phase Raman spectrum (green trace, $\lambda_{exc.}$ 514.5 nm) of trifluoroacetyl triflate.

Another significant aspect aiding in the interpretation and assignment of the spectra was the analysis of the FTIR spectra following broadband UV–visible irradiation of TFAT isolated in an Ar matrix. The matrix underwent exposure to UV–visible light for various durations (15 and 30 s, and 1, 2, 4, 7, 12, 20, 30, 50, and 80 min). Changes occurring after each irradiation period were monitored using FTIR spectroscopy. During irradiation, it was observed that the IR absorptions corresponding to the *syn–gauche* conformer increased, while those of the *syn–anti* form decreased. The final two spectra, taken after 50 and 80 min of irradiation, exhibited no further changes, indicating the system had reached a stationary state. Figure 7 illustrates selected regions of the FTIR spectrum of the matrix taken immediately after deposition and after 12 and 50 min of irradiation. These spectral

regions were chosen based on clear identification of both conformers, corresponding to the ν(C=O), ν(C−O) and δ(OCO) vibrational modes. For clarity, the spectra were normalized to the bands of the high-energy conformer. The pronounced increase in the relative intensities of the signals from the *syn–gauche* conformer compared to those of the *syn–anti* rotamer is evident in the figure.

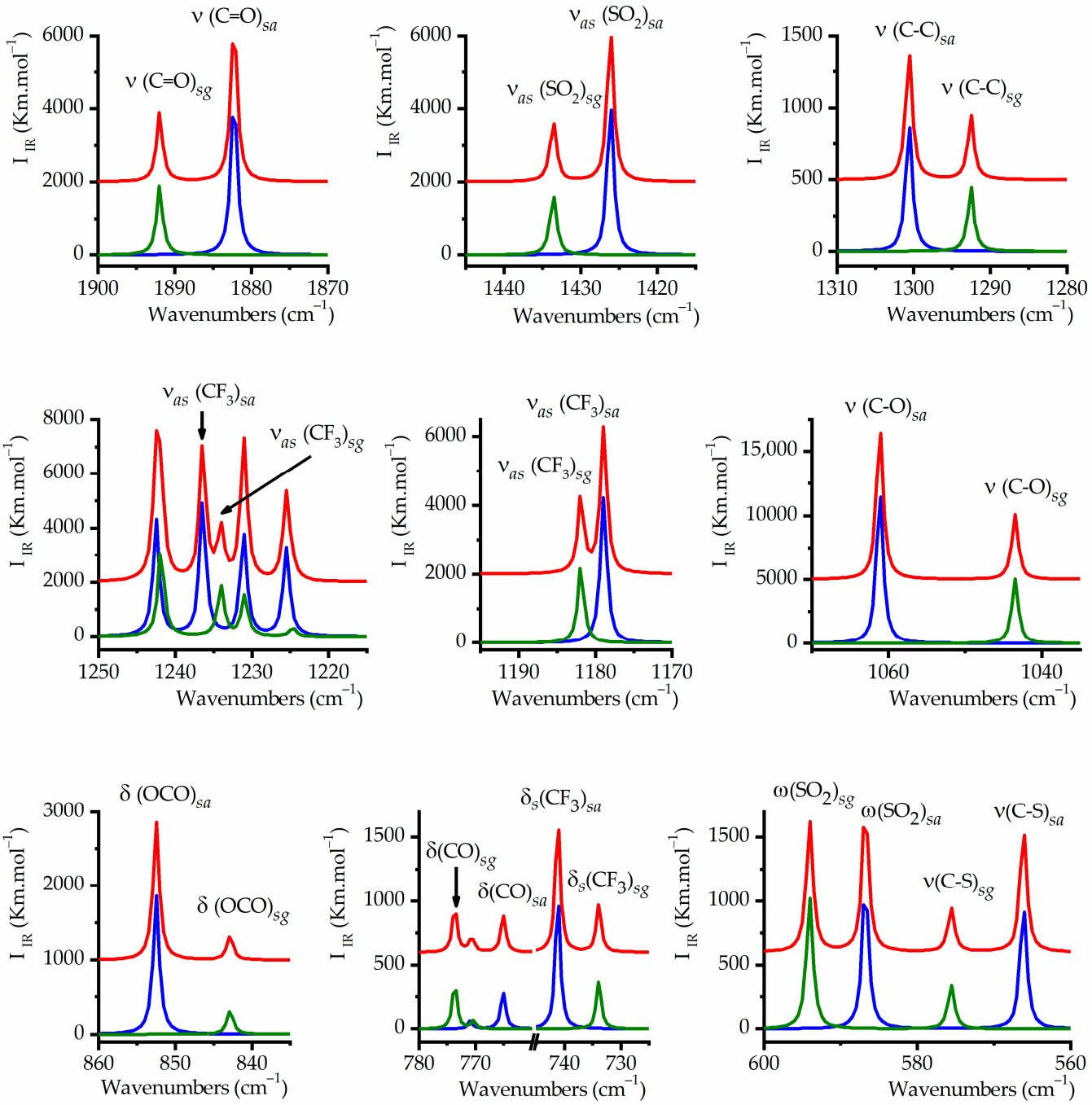

Figure 5. Simulated IR spectra in selected regions for the conformers of TFAT, scaled by their relative abundances at 25 °C, calculated with the B3LYP/cc-pvtz approximation: *syn–anti* conformer, blue spectrum scaled by 0.69 factor; *syn–gauche*, green spectrum scaled by 0.31 factor; weighted sum of the spectra of the two conformers, red spectrum, shifted on the vertical axis for clarity purposes only.

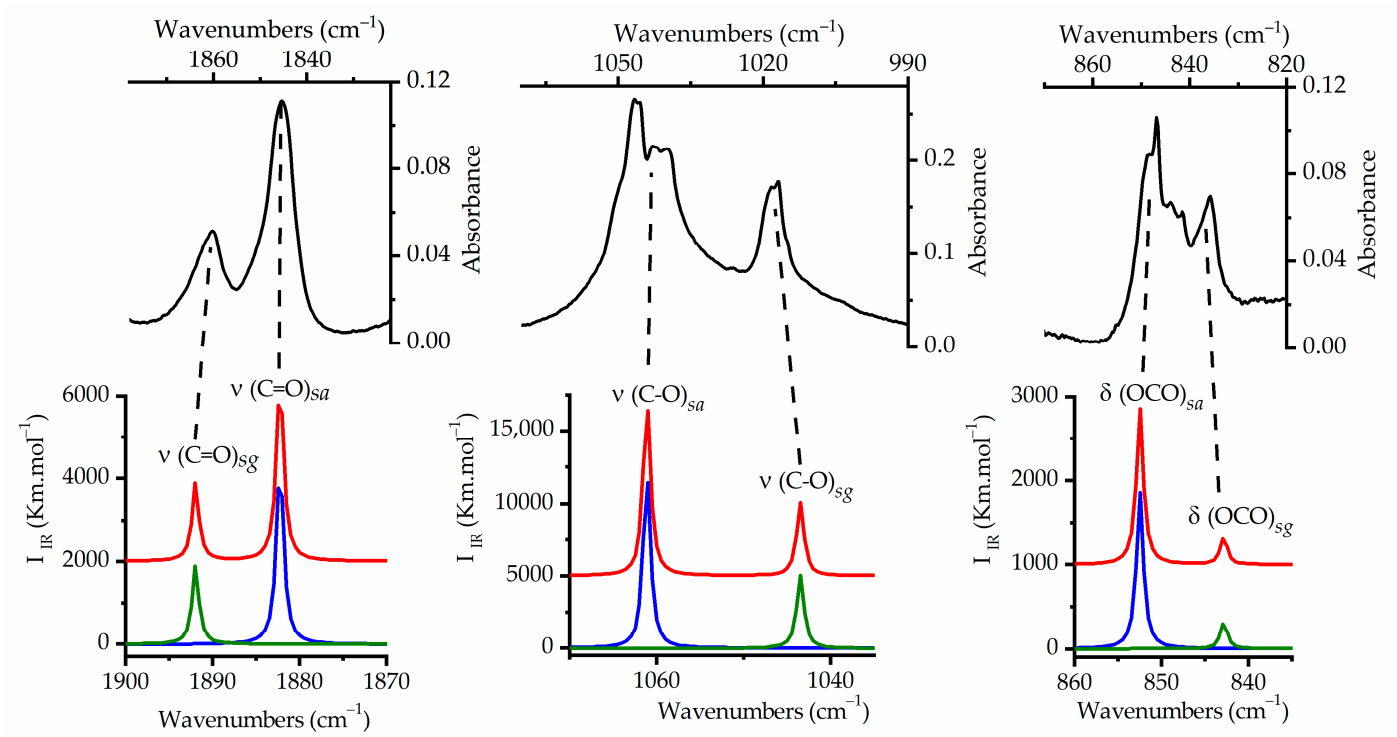

Figure 6. Comparison of the simulated IR spectra in selected regions for the conformers of TFAT, scaled by their relative abundances at 25 °C, calculated with the B3LYP/cc-pvtz approximation: *syn–anti* conformer, blue spectrum scaled by 0.69 factor; *syn–gauche*, green spectrum scaled by 0.31 factor; weighted sum of the spectra of the two conformers, red spectrum, shifted on the vertical axis for clarity purposes only and the Ar matrix FTR spectrum of TFAT (black-trace, 1:1000, 0.5 cm^{-1} resolution, 256 scans).

The abundances of the conformers were estimated from the IR matrix spectra using two different approaches. Firstly, it was assumed that in the last two spectra, taken after 50 and 80 min respectively, where a constant ratio of intensities of the bands assigned to the two conformers was achieved, the proportion of each conformer was approximately 50%, following a process known as conformational randomization. Experimental absorptivity coefficients were then calculated from the area ratio. Utilizing this relationship along with the intensity ratio in the spectrum acquired prior to irradiation, the percentage of each rotamer at room temperature was estimated. In a second method, absorptivity coefficients calculated using the B3LYP/cc-pvtz approximation were employed to correct the relationship of experimental intensities in the IR spectra of the matrix before irradiation. These procedures were performed for each of the normal modes depicted in Figure 7 (ν(C=O), ν(C−O), and δ(OCO)). Estimates between approximately 60–70% were obtained for the *syn–anti* form. The percentage determined for each normal mode using both described methods are presented in Table S5 of the Supplementary Material. Considering the various factors influencing these measurements, particularly the presence of matrix sites affecting the relative intensity of some bands, whose changes may also be influenced by irradiation, the dispersion of these values can be deemed acceptable. Moreover, they align well with the relative population predictions obtained using the B3LYP/cc-pvtz method.

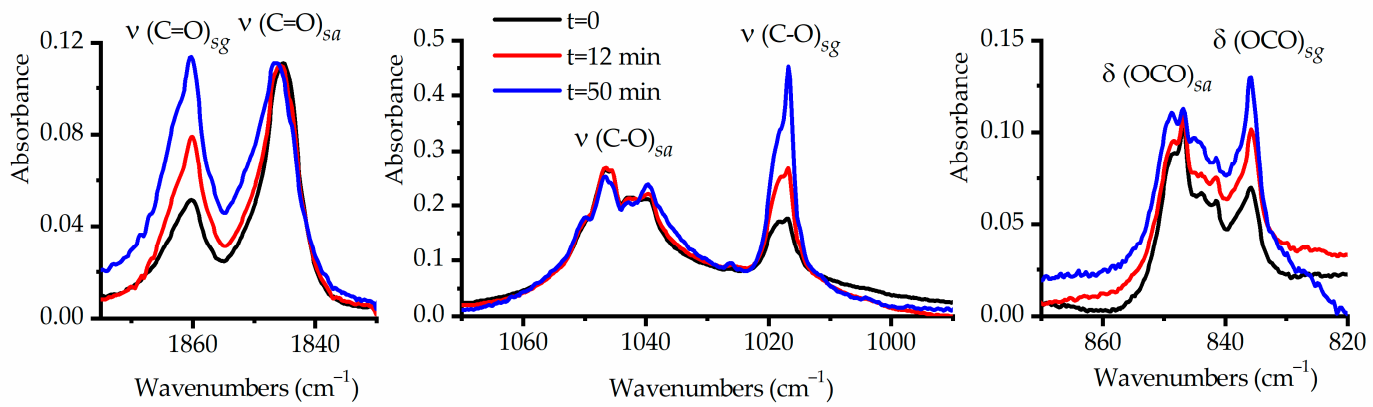

Figure 7. Selected regions of FTIR spectra of an Ar matrix containing TFAT in 1:1000 proportion: after deposition (black trace) and 12 (red trace) and 50 min (blue trace) of irradiation with broad-band UV–visible light. The spectra are normalized to the intensities of the absorption assigned to the *syn–anti* conformer, for clarity purposes only.

The experimental UV–visible gas-phase spectrum was recorded in the 190−900 nm wavelength range (see Figure S3). As predicted by TD-DFT calculations, the only electronic transition within this range, assigned to a $lp_pO \rightarrow \pi^*C{=}O$, exhibits such low intensity that it remains undetectable.

4. Conclusions

In this work, we investigate the conformers of trifluoroacetyl triflate ($CF_3C(O)OSO_2CF_3$, TFAT) using a combination of experimental vibrational spectroscopies (gas-phase FTIR, liquid-phase Raman, and Ar matrix FTIR spectroscopy) and density functional theory (DFT) calculations. The DFT calculations predict an equilibrium between two forms at ambient temperatures, with the *syn–anti* conformer (where the C=O double bond is *syn* with respect to the O−S single bond and the C−O single bond is *anti* with respect to the S−C single bond) being the preferred form, followed by the *syn–gauche* rotamer, which has a multiplicity of two.

TFAT was synthesized by reacting trifluoroacetic acid with triflic acid, using phosphorus pentoxide as the dehydrating agent. Optimal conditions to avoid secondary products were achieved using a 1:2 ratio between trifluoroacetic acid and triflic acid.

The presence of the two rotamers was experimentally detected in the Ar matrix FTIR spectra. The assignment of the FTIR bands to each form was confirmed after broadband UV–visible irradiation, as a photorotamerization process was observed. After irradiation, the bands of the more energetic form increased in intensity at the expense of those of the most abundant conformer. An approximately 60–70% of the *syn–anti* conformer at ambient temperatures was estimated from the Ar matrix spectrum of TFAT, using two different approaches to calculate the absorptivity coefficients of each conformer's band. In one case, it was assumed that approximately 50% of each form was present once the relative intensities reached a constant value after matrix irradiation. Alternatively, the absorptivity coefficients calculated with the B3LYP/cc-pvtz approximation were used. We demonstrate that both approaches lead to qualitatively similar results and that matrix-isolation FTIR spectroscopy combined with UV–visible irradiation is a valuable technique for exploring the conformational equilibrium in trifluoroacetyl triflate.

Supplementary Materials: The following supporting information can be downloaded at: https://www.mdpi.com/article/10.3390/spectroscj2020005/s1. Experimental details of the reaction between trifluoroacetyl chloride and silver triflate; Figure S1: Schematic representation of the hyperconjugative and anomeric interactions in the *syn–anti* conformer of trifluoroacetyl triflate calculated with the NBO formalism using the B3LYP/cc-pvtz approximation: (a) lpπ O → π* C=O; (b) lpσ O → σ* C=O; (c) lpσ O → σ* S=O; Figure S2: Schematic representation of the hyperconjugative and anomeric interactions in the *syn–gauche* conformer of trifluoroacetyl triflate calculated with the NBO formalism using the B3LYP/cc-pvtz approximation: (a) lpπ O → π* C=O; (b) lpσ O → σ* C=O; (c) lpσ O → σ* S−C; Figure S3: a) Experimental UV–visible spectrum of gas-phase trifluoroacetyl triflate and b) simulated electronic spectra of the *syn–anti* (blue–trace) and *syn–gauche* (green–trace) conformer of trifluoroacetyl triflate and weighted sum of the spectra of the two conformers (red–trace) calculated with the TD-B3LYP/cc-pvtz approximation; Figure S4: Schematic representation of the HOMO and LUMO orbitals of the *syn–anti* conformer of trifluoroacetyl triflate calculated with the TD-B3LYP/cc-pvtz approximation; Figure S5: Schematic representation of the HOMO and LUMO orbitals of the *syn–gauche* conformer of trifluoroacetyl triflate calculated with the TD-B3LYP/cc-pvtz approximation; Table S1: Geometrical parameters (distances in Å and angles in degrees) for the *syn–anti* and *syn–gauche* conformers of $CF_3C(O)OSO_2CF_3$ calculated with the B3LYP/cc-pvtz approximation; Table S2: Cartesian coordinates (in Å) of the *syn–anti* conformer of $CF_3C(O)OSO_2CF_3$ calculated with the B3LYP/cc-pvtz approximation; Table S3: Cartesian coordinates (in Å) of the *syn–gauche* conformer of $CF_3C(O)OSO_2CF_3$ calculated with the B3LYP/cc-pvtz approximation; Table S4: Wavenumbers, IR and Raman intensities, and tentative assignment, calculated with the B3LYP/cc-pvtz approximation for the *syn–anti* and *syn–gauche* conformers of $CF_3C(O)OSO_2CF_3$; Table S5: Percentage of the *syn–anti* conformer of $CF_3C(O)OSO_2CF_3$ estimated from the relative intensities of selected IR bands of the Ar matrix FTIR spectrum of TFAT: I) using the relationship of the absorption coefficients of the involved bands when the concentrations of the two rotamers becomes equal after the randomization process (in this case, broadband UV–visible irradiation of the matrix for 50 min); and II) through the use of the absorption coefficients obtained from the B3LYP/cc-pvtz approximation.

Author Contributions: Conceptualization, R.M.R. and C.O.D.V.; formal analysis, A.S., M.G.P. and R.M.R.; investigation, A.S. and M.G.P.; writing—original draft preparation, R.M.R.; writing—review and editing, R.M.R. and C.O.D.V.; funding acquisition, R.M.R. and C.O.D.V. All authors have read and agreed to the published version of the manuscript.

Funding: This research was funded by Consejo Nacional de Investigaciones Científicas y Técnicas (CONICET), PIP 0352 and PUE-2017-22920170100053, Agencia Nacional de Promoción Científica y Tecnológica (ANPCyT), PICT-2018-04355 and PICT-2020-03746, and Universidad Nacional de La Plata, UNLP-X822.

Institutional Review Board Statement: Not aplicable.

Informed Consent Statement: Not aplicable.

Data Availability Statement: The raw data supporting the conclusions of this article are contained within he article.

Acknowledgments: We are grateful to Luciana Tamone from the Matrix Laboratory of CEQUINOR, as well as to Gustavo Pozzi and Gino Pietrodángelo from the Raman Laboratory of CEQUINOR for their assistance during the measurements.

Conflicts of Interest: The authors declare no conflicts of interest.

References

1. López, S.E.; Restrepo, J.; Salazar, J. Trifluoroacetylation in Organic Synthesis: Reagents, Developments and Applications in the Construction of Trifluoromethylated Compounds. *Curr. Org. Synth.* **2010**, *7*, 414–432. [CrossRef]
2. Forbus, T.R.; Taylor, S.L.; Martin, J.C. Reactions of the Readily Accessible Electrophile, Trifluoroacetyl Triflate: A Very Reactive Agent for Trifluoroacetylations at Oxygen, Nitrogen, Carbon, or Halogen Centers. *J. Org. Chem.* **1987**, *52*, 4156–4159. [CrossRef]
3. Kiselyov, A.S.; Harvey, R.G. Acylation of Activated Aromatic Substrates under Mild Conditions with $(RCO)_2O/Me_2S/BF_3$. *Tetrahedron Lett.* **1995**, *23*, 4005–4008. [CrossRef]
4. Maas, G.; Stang, P.J. Dication disulfides by reaction of thioureas and related compounds with trifluoromethanesulfonic anhydride. The role of triflic anhydride as an oxidizing agent. *J. Org. Chem.* **1981**, *46*, 1606–1610. [CrossRef]

5. Michalak, R.S.; Martin, J.C. Persulfonium salts: The reaction of a difluoropersulfurane with Lewis acids. *J. Am. Chem. Soc.* **1980**, *102*, 5921–5923. [CrossRef]
6. Della Védova, C.O.; Downs, A.J.; Novikov, V.P.; Oberhammer, H.; Parsons, S.; Romano, R.M.; Zawadski, A. Fluorocarbonyl Trifluoromethanesulfonate, $FC(O)OSO_2CF_3$: Structure and Conformational Properties in the Gaseous and Condensed Phases. *Inorg. Chem.* **2004**, *43*, 4064–4071. [CrossRef] [PubMed]
7. Della Védova, C.O.; Downs, A.J.; Moschione, E.; Parsons, S.; Romano, R.M. Chlorocarbonyl Trifluoromethanesulfonate, $ClC(O)OSO_2CF_3$: Structure and Conformational Properties in the Gaseous and Condensed Phases. *Inorg. Chem.* **2004**, *43*, 8143–8149. [CrossRef]
8. Trautner, F.; Della Védova, C.O.; Romano, R.M.; Oberhammer, H. Gas phase structure and conformational properties of chlorocarbonyl trifluoromethanesulfonate, $ClC(O)OSO_2CF_3$. *J. Mol. Struct.* **2006**, *784*, 272–275. [CrossRef]
9. Romano, R.M.; Moreno Betancourt, A.; Della Vedova, C.O.; Zeng, X.; Beckers, H.; Willner, H.; Schwabedissen, J.; Mitzel, N.W. Preparation and properties of chlorosulfuryl chloroformate, $ClC(O)OSO_2Cl$. *Inorg. Chem.* **2018**, *57*, 14834–14842. [CrossRef]
10. Della Védova, C.O.; Mack, H.G. A matrix photochemistry study on (fluorocarbonyl) sulfenyl bromide: The precursor of sulfur bromide fluoride. *Inorg. Chem.* **1993**, *32*, 948–950. [CrossRef]
11. Tamone, L.M.; Picone, A.L.; Romano, R.M. New insights into the Ar-matrix-isolation FTIR spectroscopy and photochemistry of dichloroacetyl chloride, $ClC(O)CHCl_2$: Influence of O_2 and comparison with gas-phase photochemistry. *J. Photochem. Photobiol.* **2021**, *6*, 100019. [CrossRef]
12. Bava, Y.B.; Cozzarín, M.V.; Della Védova, C.O.; Willner, H.; Romano, R.M. Preparation of FC(S)SF, FC(S) SeF and FC(Se)SeF through matrix photochemical reactions of F_2 with CS_2, SCSe, and CSe_2. *Phys. Chem. Chem. Phys* **2021**, *23*, 20892–20900. [CrossRef] [PubMed]
13. Romano, R.M.; Della Vedova, C.O.; Downs, A.J.; Greene, T.M. Matrix Photochemistry of *syn*-(Chlorocarbonyl) sulfenyl Bromide, *syn*-ClC(O) SBr: Precursor to the Novel Species *anti*-ClC(O)SBr, *syn*-BrC(O)SCl, and BrSCl. *J. Am. Chem. Soc.* **2001**, *123*, 5794–5801. [CrossRef] [PubMed]
14. Forbus, T.R.; Martin, J.C. Trifluoroacetyl Triflate: An Easily Accessible, Highly Electrophilic Trifluoroacetylating Agent. *J. Org. Chem.* **1979**, *44*, 313–314. [CrossRef]
15. Taylor, S.L.; Forbus, T.R.; Martin, J.C. *Trifloroacetyl Triflate: Acetic Acid, Trifluoro-, Anhydride with Trifluoromethanesulfonic Acid. Organic Syntheses*; Kende, A.S., Freeman, J.P., Eds.; Wiley: Hoboken, NJ, USA, 2003; p. 217.
16. Taylor, S.L.; Forbus, T.R., Jr.; Martin, J.C. Trifluoroacetyl Triflate. *Org. Synth.* **1986**, *64*, 217.
17. Frisch, M.J.; Trucks, G.W.; Schlegel, H.B.; Scuseria, G.E.; Robb, M.A.; Cheeseman, J.R.; Scalmani, G.; Barone, V.; Petersson, G.A.; Nakatsuji, H.; et al. *Gaussian 09, Revision A.02*; Gaussian, Inc.: Wallingford, UK, 2016.
18. Perdew, J.P. Density-functional approximation for the correlation energy of the inhomogeneous electron gas. *Phys. Rev. B* **1986**, *33*, 8822–8824. [CrossRef] [PubMed]
19. Lee, C.; Yang, W.; Parr, R.G. Development of the Colle-Salvetti correlation-energy formula into a functional of the electron density. *Phys. Rev. B* **1988**, *37*, 785–789. [CrossRef] [PubMed]
20. Becke, A.D. Density-functional exchange-energy approximation with correct asymptotic behavior. *Phys. Rev. A* **1988**, *38*, 3098–3100. [CrossRef] [PubMed]
21. Reed, A.E.; Curtiss, L.A.; Weinhold, F. Intermolecular interactions from a natural bond orbital, donor-acceptor viewpoint. *Chem. Rev.* **1988**, *88*, 899–926. [CrossRef]
22. Glendening, E.D.; Devin, M.H.; Weinhold, F. Natural Bond Orbital Analysis of chemical structure, spectroscopy, and reactivity: How it works. In *Comprehensive Computational Chemistry*, 1st ed.; Yáñez, M., Boyd, R.J., Eds.; Elsevier: Amsterdam, The Netherlands, 2024; pp. 406–421.
23. Bauernschmitt, R.; Ahlrichs, R. Treatment of electronic excitations within the adiabatic approximation of time dependent density functional theory. *Chem. Phys. Lett.* **1996**, *256*, 454–464. [CrossRef]
24. Scuseria, G.E.; Frisch, M.J. An efficient implementation of time-dependent density-functional theory for the calculation of excitation energies of large molecules. *J. Chem. Phys.* **1998**, *109*, 8218–8224.

Disclaimer/Publisher's Note: The statements, opinions and data contained in all publications are solely those of the individual author(s) and contributor(s) and not of MDPI and/or the editor(s). MDPI and/or the editor(s) disclaim responsibility for any injury to people or property resulting from any ideas, methods, instructions or products referred to in the content.